

Muon spin relaxation and electron/neutron diffraction studies of $\text{BaTi}_2(\text{As}_{1-x}\text{Sb}_x)_2\text{O}$: Absence of static magnetism and superlattice reflections

Y. Nozaki,¹ K. Nakano,¹ T. Yajima,¹ H. Kageyama,^{1,*} B. Frandsen,² L. Liu,² S. Cheung,² T. Goko,² Y. J. Uemura,^{2,†} T. S. J. Munsie,³ T. Medina,³ G. M. Luke,³ J. Munevar,⁴ D. Nishio-Hamane,⁵ and C. M. Brown^{6,7}

¹*Department of Energy and Hydrocarbon Chemistry, Graduate School of Engineering, Kyoto University, Nishikyo, Kyoto 615-8510, Japan*

²*Department of Physics, Columbia University, 538 West 120th Street, New York, NY 10027, USA*

³*Department of Physics and Astronomy, McMaster University, 1280 Main Street West, Hamilton, Ontario, Canada L8S 4M1*

⁴*Centro Brasileiro de Pesquisas Fisicas, Rua Xavier Sigaud, 150 Urca, CEP 22290-180 Rio de Janeiro, RJ, Brazil*

⁵*Institute for Solid State Physics, University of Tokyo, 5-1-5 Kashiwanoha, Kashiwa, Chiba 277-8581, Japan*

⁶*NIST Center for Neutron Research, National Institute of Standards and Technology, 100 Bureau Drive, MS 6100, Gaithersburg, MD 20899-6100, USA*

⁷*Department of Chemical Engineering, University of Delaware, Newark, DE 19716, USA*

(Received 3 October 2013; revised manuscript received 2 November 2013; published 6 December 2013)

We present the results of muon spin relaxation/rotation, transmission electron microscopy, and neutron diffraction measurements performed on several specimens of $\text{BaTi}_2(\text{As}_{1-x}\text{Sb}_x)_2\text{O}$, which is known to have either charge density or spin density wave ordering at T_{DW} for all x , and superconductivity below $T_c \approx 1$ K for $x = 1$. Zero-field muon spin relaxation measurements show no significant increase in relaxation rate at the density wave ordering temperature for any composition, indicating that the density wave is of the charge rather than spin type. The absence of any superstructure peaks in selected area electron and high-resolution neutron diffraction measurements below T_{DW} suggests that the charge density wave does not involve modulation of atomic arrangement. Transverse field muon spin rotation measurements reveal a robust superconducting state below $T_c \approx 1$ K for $x = 1$.

DOI: [10.1103/PhysRevB.88.214506](https://doi.org/10.1103/PhysRevB.88.214506)

PACS number(s): 76.75.+i, 74.90.+n, 74.70.-b, 68.37.Og

Layered oxypnictide systems, such as $\text{ATi}_2\text{Pn}_2\text{O}$ ($A = \text{Na}_2, \text{Ba}, (\text{SrF})_2, (\text{SmO})_2$; $\text{Pn} = \text{As}, \text{Sb}, \text{Bi}$), have been found to possess interesting electronic and magnetic properties, including spin/charge density wave (S/CDW) ordering and superconductivity.¹⁻¹⁴ Although the superconducting phase transition in these systems occurs at low temperatures (≤ 5 K),⁷⁻¹¹ and in some cases not at all, they nevertheless share certain structural and electronic similarities with the cuprate and iron-pnictide compounds exhibiting high-temperature superconductivity.^{15,16} These similarities include the presence of planar sheets of Ti_2O square nets, in analogy to the CuO_2 sheets found in the cuprates, an electron configuration of $3d^1$ that is electron-hole symmetric with the $3d^9$ configuration of the cuprates, and the close proximity of the S/CDW instability to the superconducting state, as also observed in many cuprates and iron-pnictides. Given these similarities, these oxypnictide systems have the potential to yield important insights into high-temperature superconductivity.

Resistivity and magnetic susceptibility measurements recently performed on *isovalent* systems for $\text{BaTi}_2\text{Pn}_2\text{O}$, with $\text{Pn} = \text{As}^{3-}$ ($T_c = 0$ K), Sb^{3-} ($T_c = 1.2$ K), Bi^{3-} ($T_c = 4.6$ K), have revealed an intriguing phase diagram with S/CDW ordering present for $\text{BaTi}_2(\text{As}_{1-x}\text{Sb}_x)_2\text{O}$, which is quickly suppressed and replaced by a superconducting state in $\text{BaTi}_2(\text{Sb}_{1-y}\text{Bi}_y)_2\text{O}$ (Fig. 1).¹⁰ Remarkably, the superconducting phase exhibits a two-dome structure as observed in iron pnictide,¹⁷ suggesting the presence of multiple bands at the Fermi surface, in accordance with band calculations revealing contributions of $d_x^2 - y^2$, d_z^2 , and d_{xy} orbitals.¹⁸⁻²⁰ On the other hand, the hole-doped systems via *aliovalent* cation and anion substitution, $(\text{Ba}_{1-x}\text{Na}_x)\text{Ti}_2\text{Sb}_2\text{O}$ ⁸ and $\text{BaTi}_2(\text{Sb}_{1-x}\text{Sn}_x)_2\text{O}$,¹¹ respectively, display a different phase diagram with a robust

S/CDW state even while supporting superconductivity with T_c as high as 5.5 K in $(\text{Ba}_{0.67}\text{Na}_{0.33})\text{Ti}_2\text{Sb}_2\text{O}$. In addition, any two-dome structure in the superconducting state is absent, up to the experimentally available dopant level.

The observed unprecedented two-dome structure and the contrasting phase diagram that the isovalent substitution system¹⁰ exhibits in relation to the aliovalent counterpart^{8,11} signify the importance of unveiling the exact nature of the density wave ordering, either SDW or CDW, which however remains unclear even after the initial characterization of these compounds. Despite a large drop in magnetic susceptibility of $\text{Na}_2\text{Ti}_2\text{As}_2\text{O}$ at T_{DW} , a low-temperature neutron diffraction study only showed a distortion of the TiAs_4O_2 octahedron without any sign of translational symmetry breaking.²¹ Recent ^{121/123}Sb nuclear quadrupole resonance (NQR) measurements on $\text{BaTi}_2\text{Sb}_2\text{O}$ ¹² exhibited no splitting of spectrum nor appreciable broadening below T_{DW} , from which incommensurate S/CDW correlations were excluded and a commensurate CDW order was suggested, although a commensurate SDW order could not be completely ruled out. In this paper, we report muon spin relaxation/rotation (μSR) measurements for $\text{BaTi}_2(\text{As}_{1-x}\text{Sb}_x)_2\text{O}$ to confirm the absence of SDW ordering across the entire phase diagram and to examine in greater detail the low-temperature superconductivity of $\text{BaTi}_2\text{Sb}_2\text{O}$, using a dilution refrigerator to achieve temperatures as low as 30 mK. Selected area transmission electron microscopy and neutron diffraction measurements were also conducted for $\text{BaTi}_2\text{Sb}_2\text{O}$ collected above and below T_{DW} .

Four powder specimens of $\text{BaTi}_2(\text{As}_{1-x}\text{Sb}_x)_2\text{O}$ ($x = 0, 0.2, 0.6, 1$; indicated by large arrows in Fig. 1) were prepared by conventional solid-state reaction. BaO (99.99%; Aldrich), Ti (99.9%; Kojundo Chemical), As (99.9999%; Furukawa Co.,

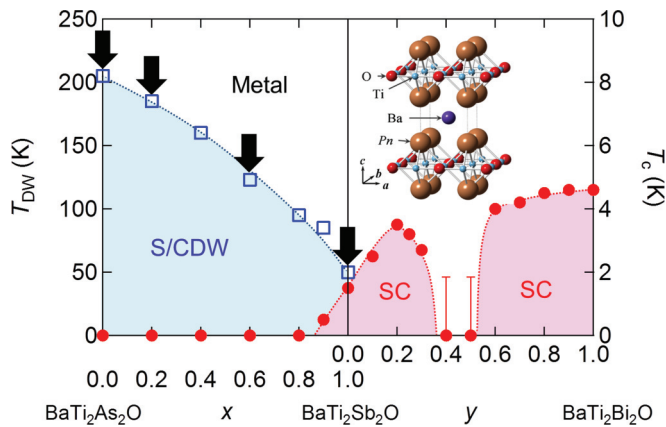


FIG. 1. (Color online) Electronic phase diagram of $\text{BaTi}_2(\text{As}_{1-x}\text{Sb}_x)_2\text{O}$ and $\text{BaTi}_2(\text{Sb}_{1-y}\text{Bi}_y)_2\text{O}$ showing the S/CDW order for $\text{BaTi}_2(\text{As}_{1-x}\text{Sb}_x)_2\text{O}$ and the two-dome structure of the superconducting state in $\text{BaTi}_2(\text{Sb}_{1-y}\text{Bi}_y)_2\text{O}$, adapted from Ref. 10. The arrows indicate the compositions studied for this paper. The inset displays the crystal structure of $\text{BaTi}_2\text{Pn}_2\text{O}$ with the space group $P4/mmm$, where the $\text{Ti}_2\text{Pn}_2\text{O}$ slabs stack in a uniform manner along the tetragonal c axis.

Ltd.), and Sb (99.9%; Kojundo Chemical) were accurately weighed according to the stoichiometric ratio and then mixed and pelletized in a nitrogen-filled dry box. The pellet was wrapped with tantalum foil, sealed in a quartz tube, and heated at 1000°C for 40 h. The laboratory x-ray diffraction (XRD) patterns, collected at room temperature using Bruker AXS D8 Advance, could be refined as the $\text{BaTi}_2\text{As}_2\text{O}$ -type structure (space group $P4/mmm$), with the linear evolution of the lattice parameters fairly consistent with the data previously reported.^{5,7,9,10}

Zero-field (ZF) μSR measurements were performed at TRIUMF in Vancouver, Canada, using the Los Alamos Meson Physics Facility (LAMPF) spectrometer, with accessible temperatures of $2\text{ K} \leq T \leq 300\text{ K}$. ZF μSR is an extremely sensitive probe of local magnetic order, and entails implanting a beam of 100% spin-polarized muons in the sample and tracking the time evolution of the polarization of the muon ensemble via the asymmetric radioactive decay of the muon into a positron and two neutrinos. In the absence of static internal magnetic order, the polarization is nonrelaxing or very slowly relaxing due to nuclear dipolar moments. On the other hand, the presence of internal magnetism causes the polarization to precess around the field if long-range order is achieved or to rapidly relax if the magnetism is not long-range ordered.

Transverse field (TF) μSR measurements were also conducted at TRIUMF to probe the superconducting state of $\text{BaTi}_2\text{Sb}_2\text{O}$, using a dilution refrigerator to cool the sample to temperatures as low as 30 mK. In a TF μSR experiment, an external magnetic field is applied perpendicular to the initial muon spin direction, causing the muon spin to precess around the vector sum of the external field and any internal field. Any relaxation of the precessing signal indicates the presence of an inhomogeneous internal field distribution. This technique is especially useful for investigating the vortex lattice phase of type-II superconductors in an external magnetic field, since the measurement of the internal field distribution provided by μSR yields direct access to microscopic details of the

superconducting state, such as the magnetic penetration depth λ . We performed our measurements under a TF of 30 mT.

Neutron diffraction measurements for $\text{BaTi}_2\text{Sb}_2\text{O}$ were performed at 2.5 K and 60 K on approximately 40 g of sample using the high-resolution neutron diffractometer ($\lambda = 1.19690\text{ \AA}$) at the National Institute of Standards and Technology (NIST) Center for Neutron Research (NCNR). Selected area electron diffraction patterns for $\text{BaTi}_2\text{Sb}_2\text{O}$ were measured at 14 K and 300 K using a JEOL 2010F transmission electron microscope (TEM) at the Institute for Solid State Physics, University of Tokyo. The sample was finely ground in methanol and then placed on Cu microgrid meshes for TEM observation.

In Fig. 2(a), we show the ZF μSR time spectra for $\text{BaTi}_2\text{As}_2\text{O}$ and $\text{BaTi}_2\text{Sb}_2\text{O}$ at temperatures above and below the density wave ordering temperature T_{DW} (200 K and 50 K, respectively). The asymmetry in the positron count between a pair of detectors, which is directly proportional to the projection of the polarization of the muon ensemble along the axis of the detector pair, is plotted along the vertical axis. For both samples, the increased relaxation of the polarization below T_{DW} is relatively slight—too small to reasonably

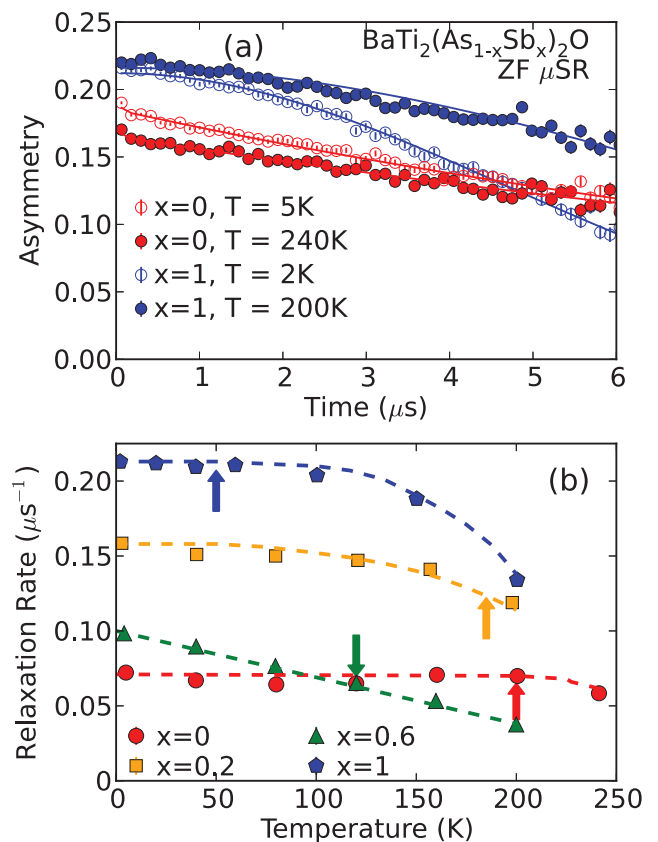


FIG. 2. (Color online) Results of zero-field muon spin relaxation measurements on $\text{BaTi}_2(\text{As}_{1-x}\text{Sb}_x)_2\text{O}$. (a) Asymmetry versus time spectra for the two end members of $\text{BaTi}_2\text{As}_2\text{O}$ and $\text{BaTi}_2\text{Bi}_2\text{O}$ showing only a moderate increase in relaxation rate at low temperatures. Error bars represent 1σ and are smaller than the symbol size. (b) Refined relaxation rates for four specimens of $\text{BaTi}_2(\text{As}_{1-x}\text{Sb}_x)_2\text{O}$. The lack of a significant increase in relaxation rate at the density wave ordering temperature excludes the possibility of SDW ordering.

attribute to SDW order. The difference in initial asymmetry of $\text{BaTi}_2\text{As}_2\text{O}$ between high and low temperatures, which may be due to muon diffusion, muonium formation at high temperatures, or a background signal from other instruments, does not signify a magnetic transition. In Fig. 2(b), we plot the temperature evolution of the relaxation rate for all samples (Gaussian decay for $x = 0.2, 1$ and exponential decay for $x = 0, 0.6$). The colored arrows indicate T_{DW} for each concentration determined by resistivity measurements.¹⁰ The absence of any significant change in relaxation rate at T_{DW} rules out the possibility of both incommensurate and commensurate SDW, thereby confirming that the density wave instability is of the charge type rather than spin type.

It is interesting that the compounds with $x = 0, 0.6$ show exponential-like relaxation of the asymmetry, while the remaining two compositions display Gaussian-like relaxation. In the absence of magnetism, weak Gaussian-like relaxation is expected due to randomly oriented nuclear moments, whereas exponential-like behavior typically indicates dilute static magnetism or fluctuating magnetic moments. In the present case, a small longitudinal field (LF) of 20 G nearly completely decouples the relaxation in the $x = 0.6$ sample, suggesting that a dilute impurity or a very weak magnetic impurity phase may exist in this sample. Although LF measurements of the $x = 0$ sample were not performed, it seems reasonable that the exponential-type behavior arises for the same reason. Also surprising is the linear behavior of the relaxation rate versus temperature exhibited by the $x = 0.6$ sample, in contrast to the other concentrations. This is possibly an extrinsic effect caused by the difficulties inherent in the solid-state synthesis of this sample. In any case, these features are far weaker than signatures expected in usual static magnetic order, and none of the compositions studied shows the dramatic change in relaxation rate expected to occur from SDW ordering.

Recently, Rohr *et al.* reported in the preprint server²² μSR experiments on the *aliovalent* solid solution

$(\text{Ba}_{1-x}\text{Na}_x)\text{Ti}_2\text{Sb}_2\text{O}$ ($0.0 \leq x \leq 0.3$) in a narrow region, where the superconducting and density wave states coexist, with T_{DW} varying only slightly. They also obtained very slow relaxation below T_{DW} , consistent with the CDW scenario. Our results on $\text{BaTi}_2(\text{As}_{1-x}\text{Sb}_x)_2\text{O}$ show that the CDW phase is stable over a wide compositional range, with T_{DW} varying from 200 K ($x = 0$) to 50 K ($x = 1$). Despite distinct phase diagrams between the two solid solutions, the CDW state is essentially the same, and its T_{DW} is tunable continuously. The combined use of the two parameters by preparing the cation/anion solid solution $(\text{Ba}_{1-x'}\text{Na}_{x'})\text{Ti}_2(\text{As}_{1-x}\text{Sb}_x)_2\text{O}$ may be an interesting possibility to optimize T_c .

From a theoretical point of view, however, both CDW and SDW states are suggested; Subedi²³ predicted a CDW instability for $\text{BaTi}_2\text{Sb}_2\text{O}$, while Singh¹⁸ and Wang *et al.*¹⁹ predicted a SDW instability for $\text{BaTi}_2\text{Sb}_2\text{O}$, and Yan and Lu²⁴ predicted a SDW instability for $\text{Na}_2\text{Ti}_2\text{Pn}_2\text{O}$. We notice that, unlike the $\text{BaTi}_2\text{Sb}_2\text{O}$ structure, with uniform stacking of the primitive cell shown in the inset of Fig. 1, the $\text{Na}_2\text{Ti}_2\text{Pn}_2\text{O}$ structure is described by the staggered stacking of successive $\text{Ti}_2\text{Pn}_2\text{O}$ slabs along the tetragonal c axis, yielding a body-centered cell. So far, superconductivity has been observed only in the compounds with the $\text{BaTi}_2\text{Sb}_2\text{O}$ -type structure, suggesting that the stacking manner of the $\text{Ti}_2\text{Pn}_2\text{O}$ slabs (staggered or uniform) may exert a crucial influence on the nature of the density wave and ultimately the appearance of superconductivity. Interestingly, superconductivity is absent in $(\text{SrF})_2\text{Ti}_2\text{Bi}_2\text{O}$ with the body-centered cell, even though no density wave anomaly is observed in resistivity and susceptibility.⁹ Therefore, we consider that whether or not the CDW state is the only density wave state in the whole family of $\text{ATi}_2\text{Pn}_2\text{O}$ is still an open issue.

In order to probe the structural change upon the CDW transition, we performed a high-resolution powder neutron diffraction study on $\text{BaTi}_2\text{Sb}_2\text{O}$ at 60 K and 2.5 K (see Fig. 3). We do not observe any splitting of peaks, nor

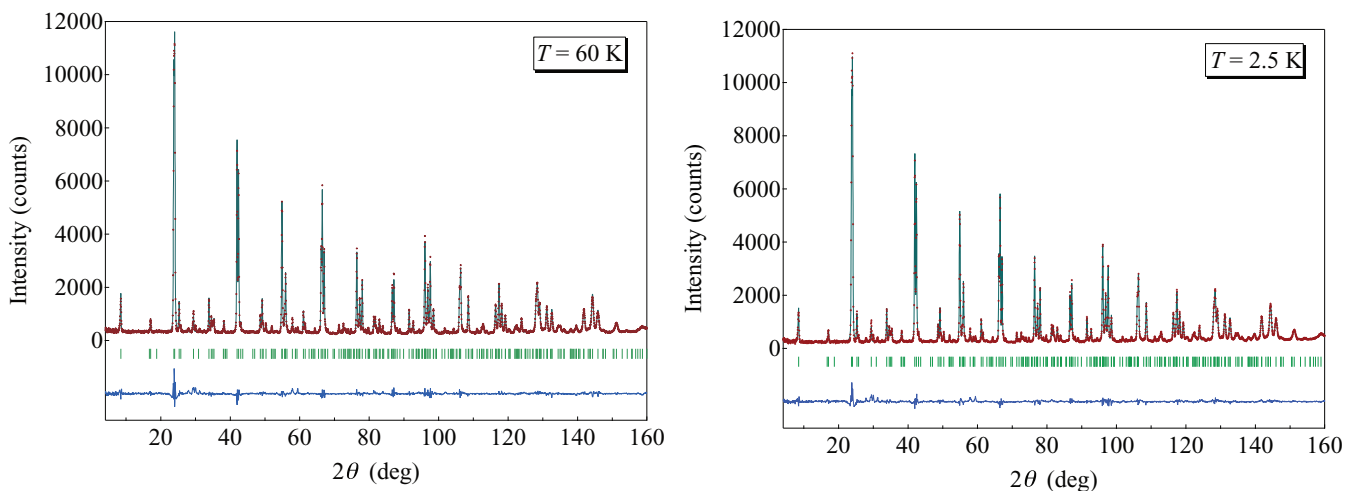


FIG. 3. (Color online) Neutron diffraction patterns at 60 K (left) and 2.5 K (right), showing observed (red circle), calculated (green line), and difference (blue line) profiles. Space group $P4/mmm$, with Ba on $1d$, Ti on $2f$, Sb on $2g$ ($0,0,z$), and O on $1c$, with 100% occupation. Refined parameters and goodness-of-fit factors for 60 K [2.5 K] are $a = 4.1069(2)$ [$4.10711(4)$] Å, $c = 8.0517(4)$ [$8.0482(1)$] Å, $z = 0.7520(2)$ [$0.7519(2)$] Å, $100U_{\text{iso}} = 0.28(3)$ [$0.16(3)$] Å² for Ba, $0.36(2)$ [$0.35(2)$] Å² for Ti, $0.43(2)$ [$0.41(2)$] Å² for Sb, $0.43(3)$ [$0.40(3)$] Å² for O, $R_w = 7.073$ [7.530]%, $R_p = 4.963$ [4.994]%. Values in parentheses represent one standard deviation of the fit parameter.

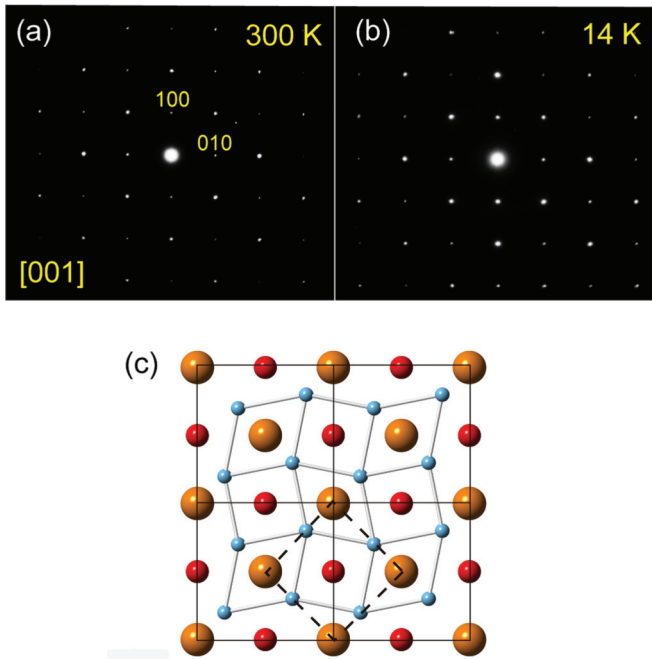


FIG. 4. (Color online) Selected area electron diffraction patterns from [001] for BaTi₂Sb₂O at (a) 300 K and (b) 14 K, showing the absence of superstructure below T_{DW} . (c) A proposed $\sqrt{2} \times \sqrt{2} \times 1$ superstructure as a result of CDW transition,²³ where the blue, red, and brown spheres denote, respectively, Ti, O, and Sb. The unit cell of the original structure is shown by the broken lines.

superreflections, in the diffraction pattern at 2.5 K, and the Rietveld refinement of structural models for both patterns does not provide any notable difference. It is rather surprising that even TEM did not reveal any superreflection peaks (see Fig. 4 and Supplemental Material²⁵). This apparently contradicts the theoretically predicted $\sqrt{2} \times \sqrt{2} \times 1$ superstructure [Fig. 4(c)], with a coherent distortion corresponding to elongation or compression of the Ti squares without an enclosed O such that the Ti squares with O rotate either clockwise or counterclockwise.²³ On the other hand, the Sb-NQR spectra below T_{DW} clearly exhibit a breaking of 4-fold rotation symmetry around Sb nuclei.¹² Accordingly, the CDW transition gives only electron modulation, while the atomic positions remain unchanged, at least within the instrumental resolution of the present TEM equipment.

To investigate the superconducting state of BaTi₂Sb₂O, we used a dilution refrigerator to cool the specimen to 30 mK under an external magnetic field of magnitude 0.03 T and collected TF μ SR time spectra at several temperatures up to 1.6 K. Figure 5(a) displays the spectra at $T = 1.2$ K and 30 mK, showing a clear increase in relaxation at low temperature due to the formation of the vortex lattice in the superconducting state. Over half the total asymmetry, however, remains essentially nonrelaxing, even at low temperature, because a large portion of the incident muons were implanted in the nonsuperconducting silver sample holder. The very slight relaxation evident at $T = 1.2$ K arises from nuclear dipolar moments and is assumed to be temperature independent, adding in quadrature to the Gaussian relaxation rate due to the vortex lattice. This superconductivity-induced muon relaxation rate σ_{sc} , which

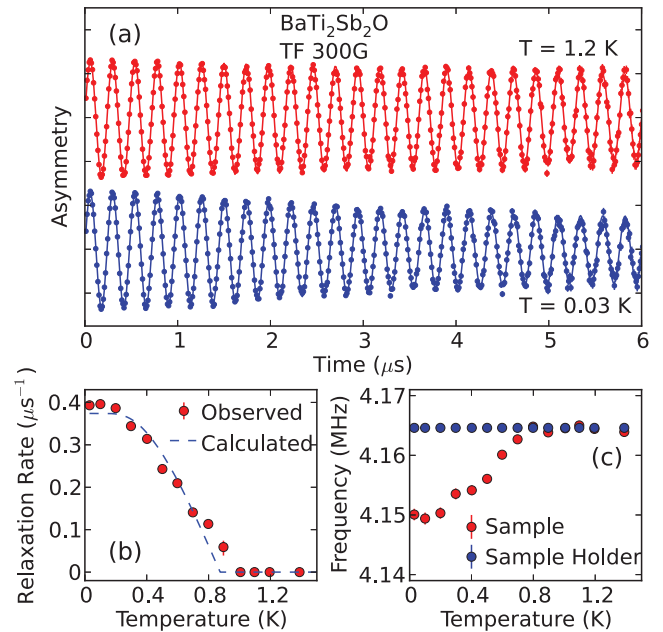


FIG. 5. (Color online) Results of TF muon spin rotation measurements on BaTi₂Sb₂O. (a) Asymmetry versus time spectra at two different temperatures. The increased damping of the oscillating signal is due to the presence of the vortex lattice in the superconducting state. (b) Observed and calculated temperature evolution of the superconducting relaxation rate σ_{sc} . The calculated best fit assumes an isotropic BCS superconductor in the weak coupling limit. (c) The temperature evolution of the precession frequency showing a decrease in frequency below T_c .

is proportional to the penetration depth as λ^{-2} , is plotted for several temperatures in Fig. 5(b), showing robust bulk superconductivity below the critical temperature $T_c \approx 1$ K. At $T = 30$ mK, $\sigma_{sc} = 0.393 \pm 0.007 \mu\text{s}^{-1}$, corresponding to $\lambda = 4310 \pm 40 \text{ \AA}$ using an empirical conversion factor (see Supplemental Material).²⁶ The oscillation frequency as a function of temperature is plotted in Fig. 4(c), demonstrating the decrease in frequency below T_c characteristic of many type-II superconductors.

To obtain further information about the superconducting state, we attempted to fit a Bardeen Cooper Schreffer (BCS) s -wave model in the weak coupling limit to the observed temperature dependence of $\sigma_{sc}(T)$. The best-fit curve, corresponding to $T_c = 0.87 \pm 0.03$ K and $\sigma_{sc}(T = 0) = 0.37 \pm 0.01 \mu\text{s}^{-1}$, is shown as the blue broken line in Fig. 4(b). One might speculate that the inability of the fit to capture the full shape of the observed $\sigma_{sc}(T)$ may be due to anisotropy in the superconducting gap. Alternatively, if there are multiple bands crossing the Fermi surface as previously suggested, we could be observing the effect of multiple superconducting gaps. However, we note that a careful study of the field dependence of $\sigma_{sc}(T)$ should be conducted to further investigate this point, along with additional studies using single-crystal specimens and better statistics.

In summary, we have reported ZF and TF μ SR measurements on BaTi₂(As_{1-x}Sb_x)₂O ($x = 0, 0.2, 0.6, 1$) in conjunction with selected area electron and high-resolution

neutron diffraction measurements. The lack of significant low-temperature relaxation in ZF μ SR excludes the possibility of SDW ordering, indicating that the previously observed anomaly in the resistivity is due to CDW ordering, in accordance with the Sb-NQR results. The absence of split peaks or superreflections in the diffraction measurements suggests that the CDW state exists only as a small but finite modulation of the electron density, without any accompanying long-range structural modulation of the atoms. TF μ SR measurements on BaTi₂Sb₂O reveal a robust superconducting state below $T_c \approx 1$ K, with the lowest-temperature penetration depth approximately 4300 Å. High-quality single-crystal specimens should be prepared to further study the details of the pairing symmetry and the relationship between the CDW and superconducting phases observed in this system.

This work was supported by the FIRST program, Japan Society of the Promotion of Science (JSPS). The work at Columbia and TRIUMF was supported by the US National Science Foundation PIRE (Partnership for International Research and Education: OISE-0968226) and DMR-1105961 projects, the Japan Atomic Energy Agency (JAEA) Reimei project, and by a travel support grant from the Friends of Todai, Inc., to Nozaki, Frandsen, Cheung, and Liu. The work at McMaster was supported by The National Sciences and Engineering Research of Canada (NSERC) and The Canadian Institute for Advanced Research (CIFAR). Certain commercial products are identified in this paper to foster understanding; such identification does not imply recommendation or endorsement by the NIST, nor does it imply that the materials or equipment identified are necessarily the best available for the purpose.

*kage@scl.kyoto-u.ac.jp

†tomo@lorentz.phys.columbia.edu

¹A. Adam and H.-U. Z. Schuster, *Anorg. Allg. Chem.* **584**, 150 (1990).

²E. A. Axtell, III, T. Ozawa, S. M. Kauzlarich, and R. R. P. Singh, *J. Solid State Chem.* **134**, 423 (1997).

³R. H. Liu, Y. A. Song, Q. J. Li, J. J. Ying, Y. J. Yan, Y. He, and X. H. Chen, *Chem. Mater.* **22**, 1503 (2010).

⁴R. H. Liu, D. Tan, Y. A. Song, Q. J. Li, Y. J. Yan, J. J. Ying, Y. L. Xie, X. F. Wang, and X. H. Chen, *Phys. Rev. B* **80**, 144516 (2009).

⁵X. F. Wang, Y. J. Yan, J. J. Ying, Q. J. Li, M. Zhang, N. Xu, and X. H. Chen, *J. Phys.: Condens. Matter* **22**, 075702 (2010).

⁶T. C. Ozawa and S. M. Kauzlarich, *Chem. Mater.* **13**, 1804 (2001).

⁷T. Yajima, K. Nakano, F. Takeiri, T. Ono, Y. Hosokoshi, Y. Matsushita, J. Hester, Y. Kobayashi, and H. Kageyama, *J. Phys. Soc. Jpn.* **81**, 103706 (2012).

⁸P. Doan, M. Gooch, Z. Tang, B. Lorenz, A. Moller, J. Tapp, P. C. W. Chu, and A. M. Guloy, *J. Am. Chem. Soc.* **134**, 16520 (2012).

⁹T. Yajima, K. Nakano, F. Takeiri, J. Hester, T. Yamamoto, Y. Kobayashi, N. Tsuji, J. Kim, A. Fujiwara, and H. Kageyama, *J. Phys. Soc. Jpn.* **82**, 013703 (2013).

¹⁰T. Yajima, K. Nakano, F. Takeiri, Y. Nozaki, Y. Kobayashi, and H. Kageyama, *J. Phys. Soc. Jpn.* **82**, 033705 (2013).

¹¹K. Nakano, T. Yajima, F. Takeiri, M. A. Green, J. Hester, Y. Kobayashi, and H. Kageyama, *J. Phys. Soc. Jpn.* **82**, 074707 (2013).

¹²S. Kitagawa, K. Ishida, K. Nakano, T. Yajima, and H. Kageyama, *Phys. Rev. B* **87**, 060510(R) (2013).

¹³M. Gooch, P. Doan, Z. Tang, B. Lorenz, A. M. Guloy, and P. C. W. Chu, *Phys. Rev. B* **88**, 064510 (2013).

¹⁴A. P. Litvinchuk, P. Doan, Z. Tang, and A. M. Guloy, *Phys. Rev. B* **87**, 064505 (2013).

¹⁵K. Ishida, Y. Nakai, and H. Hosono, *J. Phys. Soc. Jpn.* **78**, 062001 (2009).

¹⁶T. Tohyama, *Jpn. J. Appl. Phys.* **51**, 010004 (2012).

¹⁷S. Iimura, S. Matuishi, H. Sato, T. Hanna, Y. Muraba, S. W. Kim, J. E. Kim, M. Takata, and H. Hosono, *Nat. Commun.* **3**, 943 (2012).

¹⁸D. J. Singh, *New J. Phys.* **14**, 123003 (2012).

¹⁹G. Wang, H. Zhang, L. Zhang, and C. Liu, *J. Appl. Phys.* **113**, 243904 (2013).

²⁰D. V. Suetin and A. L. Ivanovskii, *J. Alloys Compd.* **564**, 117 (2013).

²¹T. C. Ozawa, R. Pantoja, E. A. Axtell, III, S. M. Kauzlarich, J. E. Greedan, M. Bieringer, and J. W. Richardson, Jr., *J. Solid State Chem.* **153**, 275 (2000).

²²F. v. Rohr, A. Schilling, R. Nesper, C. Baines, and M. Bendele, *Phys. Rev. B* **88**, 140501(R) (2013).

²³A. Subedi, *Phys. Rev. B* **87**, 054506 (2013).

²⁴X.-W. Yan and Z.-Y. Lu, *J. Phys.: Condens. Matter* **25**, 365501 (2013).

²⁵See Supplemental Material at <http://link.aps.org/supplemental/10.1103/PhysRevB.88.214506> for neutron diffraction patterns for BaTi₂Sb₂O at 60 K and 2.5 K and refined parameters.

²⁶Y. J. Uemura, A. Keren, G. M. Luke, L. P. Le, B. J. Sternlieb, W. D. Wu, J. H. Brewer, R. L. Whetten, S. M. Huang, S. Lin, R. B. Kaner, F. Diederich, S. Donovan, G. Guner, and K. Holczer, *Nature* **352**, 605 (1991).